



## Ultraselective carbon molecular sieve membrane for hydrogen purification

Ruisong Xu<sup>a</sup>, Liu He<sup>a</sup>, Lin Li<sup>a</sup>, Mengjie Hou<sup>a</sup>, Yongzhao Wang<sup>b,c</sup>, Bingsen Zhang<sup>b,c</sup>,  
Changhai Liang<sup>a</sup>, Tonghua Wang<sup>a,\*</sup>

<sup>a</sup>State Key Laboratory of Fine Chemicals, Group of Carbon Membranes and Porous Materials, School of Chemical Engineering, Dalian University of Technology, Dalian 116024, Liaoning, China

<sup>b</sup>Shenyang National Laboratory for Materials Science, Institute of Metal Research, Chinese Academy of Sciences, Shenyang 110016, Liaoning, China

<sup>c</sup>School of Materials Science and Engineering, University of Science and Technology of China, Shenyang 110016, Liaoning, China

### ARTICLE INFO

#### Article history:

Received 10 January 2020

Revised 27 February 2020

Accepted 2 March 2020

Available online 8 March 2020

#### Keywords:

Hydrogen separation and purification

Carbon molecular sieve membrane

Ultrahigh selectivity

High-purity hydrogen

### ABSTRACT

Hydrogen is a green clean fuel and chemical feedstock. Its separation and purification from hydrogen-containing mixtures is the key step in the production of hydrogen with high purity (>99.99%). In this work, carbon molecular sieve (CMS) membranes with ultrahigh permselectivity for hydrogen purification were fabricated by high-temperature (700–900 °C) pyrolysis of polymeric precursor of phenolphthalein-based cardo poly (arylene ether ketone) (PEK-C). The evolution of the microstructural texture and ultramicroporous structure and gas separation performance of the CMS membrane were characterized via TG-MS, FT-IR, XRD, TEM, CO<sub>2</sub> sorption analysis and gas permeation measurements. CMS membranes prepared at 700 °C exhibited amorphous turbostratic carbon structures and high H<sub>2</sub> permeability of 5260 Barrer with H<sub>2</sub>/CH<sub>4</sub>, H<sub>2</sub>/N<sub>2</sub> and H<sub>2</sub>/CO selectivities of 311, 142, 75, respectively. When carbonized at 900 °C, the CMS membrane with ultrahigh H<sub>2</sub>/CH<sub>4</sub> selectivity of 1859 was derived owing to the formation of the dense and ordered carbon structure. CMS membranes with ultrahigh permselectivity exhibit an attractive application prospect in hydrogen purification.

© 2020 Science Press and Dalian Institute of Chemical Physics, Chinese Academy of Sciences. Published by Elsevier B.V. and Science Press. All rights reserved.

### 1. Introduction

Hydrogen, as a basic chemical feedstock, is widely used to produce various petrochemical products needed in our daily life. With the growing demand of global energy and environmental protection, hydrogen energy has been considered as one of the most promising alternatives to traditional fossil fuels and offer the potential to effectively alleviate the serious energy crisis and greenhouse effect owing to its distinct advantages such as abundant sources, high energy density and clean combustion without carbon emission [1]. Furthermore, Hydrogen-based fuel cell as an important energy carrier have great potential for large-scale applications due to its high efficiency and environmental friendliness [2]. The widespread use of hydrogen has motivated the advent of the “hydrogen economy” era and the growing demand for hydrogen [3]. Currently, hydrogen is mainly manufactured from fossil fuels using the technologies of steam reforming of natural gas and

coal gasification following with water-gas shift processes [3,4]. The hydrogen recovered from industrial tail gases such as ammonia plant purge gas and coke oven gas from steel plants is another considerable source [5–7]. Whichever method is adopted to produce hydrogen, the separation and purification of hydrogen is the key step to meet the purity requirements of various hydrogen applications because hydrogen products inevitably contain many impurities, methane, nitrogen, carbon monoxide, carbon dioxide, water and light hydrocarbons, etc. [3,8]. Especially, high purity (>99.99%) of hydrogen is required for the applications of fuel cells, semiconductor manufacture and rocket engine fuels [2,3].

Three main approaches can be used for hydrogen purification, including pressure swing adsorption, cryogenic distillation and membrane separation technology [9–11]. Membrane technology is regarded as an attractive alternative to the other two conventional separation techniques with high energy consumption owing to high energy efficiency, low operational cost, and good environmental compatibility [8]. Many efforts have been made in the development of advance membrane materials for hydrogen purification such as dense metallic membranes, polymeric membranes, micro-

\* Corresponding author.

E-mail address: [wangth@dlut.edu.cn](mailto:wangth@dlut.edu.cn) (T. Wang).



**Fig. 1.** Chemical structure of PEK-C polymer and three-dimensional conformational structure of the polymeric chain simulated by Materials Studio<sup>TM</sup>.

porous inorganic membranes, metal organic frameworks (MOFs) membranes and carbon-based membranes [3,4,11,12]. To date, however, only a small number of polymeric membranes have been commercialized in hydrogen separation applications, for example, polysulfone, silicone rubber, polyimide and cellulose acetate [3]. Polymeric membranes are generally faced with the challenges of low gas permeability as well as low thermal and chemical corrosion resistance, which restricts their widespread applications.

Carbon molecular sieve (CMS) membranes, as a kind of carbon-based membrane materials, are fabricated from the pyrolysis and carbonization of polymeric precursors under controlled conditions [12–14]. CMS membranes include the pure carbon membranes (or unsupported) and supported carbon membranes. The former are often used on a laboratory scale to study the intrinsic properties of polymeric precursors and gas separation performance of CMS membranes, and the latter that are manufactured on a porous support such as ceramic and metallic disk or tube are more favorable in commercial application due to the improved mechanical property [15]. Compared to polymeric membranes, CMS membranes exhibit higher thermal and chemical stabilities and better plasticization resistance. CMS membranes also have excellent gas separation performance for hydrogen purification, which can exceed the Robeson upper bounds of polymeric membranes that plot a trade-off relationship between gas permeability and selectivity [14,16]. The gas permeation performance of CMS membranes is mainly affected by the two critical parameters of polymeric precursors and final treatment temperature [13,17–21]. Many polymeric precursors were used to prepare CMS membranes, including aromatic polyimide and derivatives [22–24], polyetherimide [25], phenolic resin [26], poly(furfuryl alcohol) [27], polyphenylene oxide [28], poly(phthalazinone ether sulfone ketone) [29,30]. For instance, Ma et al. used an intrinsically microporous polyimide to prepare CMS membranes, and the membrane treated at 630 °C possessed H<sub>2</sub> permeability of 4690 Barrer with the H<sub>2</sub>/CH<sub>4</sub> selectivity of 81 [31]. Chen et al. selected a simple glucose as the precursor for CMS membrane, which was inspired from cooking, and found that the obtained CMS membrane exhibited ultrahigh H<sub>2</sub> permeability of 8705 Barrer with the H<sub>2</sub>/CH<sub>4</sub> and H<sub>2</sub>/N<sub>2</sub> selectivities of 9.9 and 11.6, respectively [32]. However, the gas permselectivities of CMS membranes prepared are commonly not high enough to meet the requirements of commercial applications [16]. Therefore, great efforts should be devoted to developing novel polymeric precursors to prepare CMS membranes with high gas permeability and high selectivity, considering that high permeability is beneficial to reduce investment costs and high selectivity will meet the demand for high purity.

Phenolphthalein-based cardo poly(arylene ether ketone) (PEK-C) is a commercially available polymer with good membrane-forming property, high thermal stability and high fraction free volume (FFV ~ 0.159), in which the pendant cardo groups twist molecular chains into a helical structure and reduce chain packing efficiency, as shown in Fig. 1. All these features make PEK-

C polymer suitable membrane material for gas separation. In our previous work, PEK-C polymer was selected to prepare thermal crosslinking membranes at the heat treatment temperature of 400–475 °C, and showed an attractive prospect in gas separation membrane materials [33]. In the present study, the PEK-C polymer was used for the first time to prepare ultraselective CMS membranes for hydrogen purification. The gas separation performance of CMS membranes for H<sub>2</sub>/CH<sub>4</sub>, H<sub>2</sub>/CO and H<sub>2</sub>/N<sub>2</sub> gas pairs was tuned via rationally controlling the final pyrolysis temperature. The structural evolution of carbon during thermal treatment and the micromorphology and ultramicroporous structure of CMS membranes were investigated.

## 2. Experimental

### 2.1. Materials

The PEK-C polymeric precursor was provided by Xuzhou (Jiangsu, China) Engineering Plastics Co., Ltd. N,N-dimethylacetamide (DMAc, analytical grade) was purchased as a solvent from Tianjin (China) Kermel Chemical Reagent. High-purity (99.99%) gases of H<sub>2</sub>, N<sub>2</sub>, CO, and CH<sub>4</sub> were purchased from Dalian (Liaoning, China) gas company.

### 2.2. Preparation of CMS membranes

Dense PEK-C polymeric membranes were firstly prepared by evaporating 17 wt% polymer/DMAc solution on a leveled heating plate at 40 °C under a dry and dust-free environment. The fresh membranes obtained were then heated in a vacuum oven at 100 °C and 150 °C for 24 h to remove the residual solvent. The detailed preparation process can be found in our previous work [33]. The resulting PEK-C polymeric membranes (65–75 μm) were cut into 1.5 × 1.5 cm<sup>2</sup> pieces and used to prepare CMS membranes.

Before carbonization, the PEK-C polymeric precursors need to undergo an oxidative pretreatment to prevent the membranes from melting during thermal treatment [33]. The pretreatment was carried out in a muffle furnace under a 200 mL/min of air flow. The furnace temperature was ramped at 3 °C/min from room temperature to 370 °C, and then held isothermally for 30 min. After the heating procedure was completed, the pretreated membranes were immediately removed from the furnace and rapidly cooled to room temperature.

The pretreated membranes were further carbonized in a tubular furnace under N<sub>2</sub> atmosphere, which were heated at a ramp rate of 3 °C/min from room temperature to the target temperature (700–900 °C) and then held isothermally for 60 min. Thereafter, the furnace was naturally cooled to room temperature. The prepared carbon molecular membranes with the thickness of 55–65 μm were named as “CMS-T”, where “T” represents the final carbonization temperature. To avoid the influence of physical aging [34,35], the

gas permeation properties of the obtained CMS membranes were immediately tested after taking out from the furnace.

### 2.3. Characterizations

To explore the CMS structural evolution during pyrolysis, the thermal decomposition behavior of PEK-C polymeric precursor was monitored via a Thermal Gravimetric analyzer (TA, SDT650) and Mass Spectrometer (OMNI STAR-GSD320) (TGA-MS). Samples were heated from room temperature to 900 °C at 10 °C/min, and argon gas was employed as the atmosphere and carrier gas. Fourier transform infrared spectra (FT-IR) of membranes were obtained using a Fourier infrared spectrometer (Bruker, EQUINOX55). Wide-angle X-ray diffraction (WAXD) spectra of CMS membranes were measured via an XRD diffractometer (Rigaku, D/max-2400) to investigate the microstructures of membranes. And a transmission electron microscope (TEM) (FEI, Tecnai G2 F20) was used to explore the morphology and fine structures of CMS membranes. CO<sub>2</sub> sorption isotherms of CMS membranes were detected using an auto-adsorption apparatus (Quantachrome, iQ2) at 0 °C. Samples were degassed at 250 °C for 5 h under vacuum condition prior to the adsorption measurements. The corresponding pore size and distribution was calculated by the non-local density functional theory (NLDFT) model.

### 2.4. Measurements of gas permeation properties

The single and mixed gas permeation properties of CMS membranes were detected by a gas permeation equipment made in our lab and using the variable volume-constant pressure method. The detailed information can be found in our previous works [36]. The feed gas pressure was 0.01 MPa, and the flow rate was 10 ml/min. The permeated gases were sent to a gas chromatography equipment (FULI, 9790II) for analysis with a sweep gas (Argon) of 2 mL/min. The binary gas mixtures used in this work such as H<sub>2</sub>/CO, H<sub>2</sub>/N<sub>2</sub> and H<sub>2</sub>/CH<sub>4</sub> were prepared by a home-made mixing device, and the concentration of each component of the resulting mixtures was stable and reach to 50 vol%. At least three samples from each group were measured to obtain the representative data.

The gas permeability ( $P$ ) of CMS membrane can be expressed as the product of the diffusion coefficient ( $D$ ) and the sorption coefficient ( $S$ ), and can also be calculated by the Eq. (1), where  $F$  refers to the permeating gas flux (cm<sup>3</sup>/s),  $l$  is the membrane thickness (cm),  $A$  is the effective area of membrane (cm<sup>2</sup>),  $\Delta p$  refers to the pressure drop from the feed side to the permeate side (cmHg).

$$P = D \times S = \frac{Fl}{A\Delta p} \quad (1)$$

Gas sorption measurements were conducted at 30 °C and at pressures ranging from 0.5 kPa to 100 kPa. Before sorption, samples were degassed for 12 h in vacuum. For rigid and porous CMS materials, the sorption isotherms are usually defined by the Langmuir isotherm, as shown in Eq. (2).

$$C = \frac{C_0 bp}{1 + bp} \quad (2)$$

where  $C$  is the equilibrium sorption capacity (cm<sup>3</sup>(STP)/cm<sup>3</sup>(CMS)),  $C_0$  represents the saturated Langmuir sorption capacity (cm<sup>3</sup>(STP)/cm<sup>3</sup>(CMS)),  $b$  refers to the Langmuir affinity constant (1/kPa), and  $p$  is the partial pressure (kPa).

The sorption coefficient ( $S$ ) of the penetrant at a given pressure can be calculated according to the Langmuir isotherms, as expressed in Eq. (3), where  $p_i$  is the pressure used in the permeation measurements.

$$S = \frac{C}{p_i} = \frac{C_0 b}{1 + bp_i} \quad (3)$$

Therefore, the diffusion coefficient ( $D$ ) can be given by the ratio of the permeability and the sorption coefficient, as shown in Eq. (4).

$$D = \frac{P}{S} \quad (4)$$

The ideal gas selectivity ( $\alpha_{A/B}$ ) for penetrants A and B, is calculated by the ratio of  $P_A$  and  $P_B$ , and can also be divided into the diffusion selectivity and the sorption selectivity, as illustrated in Eq. (5).

$$\alpha_{A/B} = \frac{P_A}{P_B} = \frac{D_A}{D_B} \cdot \frac{S_A}{S_B} \quad (5)$$

The selectivity of mixed gases is calculated by the Eq. (6), where  $x$  and  $y$  are the mole fraction of component A or B in the feed side and permeate side, respectively.

$$\alpha_{A/B} = \frac{y_A/y_B}{x_A/x_B} \quad (6)$$

Operating temperature dependence of pure gas permeabilities for CMS membranes were measured at temperature range of 30–50 °C. An Arrhenius relationship is commonly used to describe the temperature dependence of gas permeability. The Arrhenius equation can be represented as the following pattern (7):

$$\ln P = \ln P_0 - \frac{E_p}{RT} \quad (7)$$

where  $P_0$  refers to the pre-exponential factor,  $E_p$  is the permeation activation energy (kJ/mol),  $R$  represents the universal gas constant (J/mol K), and  $T$  is the absolute temperature. By plotting the curve of  $\ln P$  versus  $1/T$ ,  $E_p$  can be obtained according to the slope of the fitting line.

## 3. Results and discussion

### 3.1. Chemical structural evolution during thermal treatment

Fig. 2(a) illustrated that the weight loss of PEK-C polymeric precursor started to occur at around 400 °C. In the temperature range of 400–650 °C, the weight loss was the largest and accounted for 36.4% of the total weight, which was the main stage of polymer pyrolysis. Many thermal decomposition reactions might take place during this stage. According to our previous reports [33], the weight loss before 500 °C was mainly attributed to the thermal decomposition of the pendant cardo groups accompanying with releasing CO<sub>2</sub> (Fig. 2(b)), which resulted in the formation of the biphenyl cross-linkages between molecular chains and enlargement of interchain distance. When the temperature was above 500 °C, the polymeric main chains pyrolyzed and released small gas molecules such as CO<sub>2</sub>, CO, H<sub>2</sub>O, and H<sub>2</sub>. The FT-IR spectra (Fig. 3) showed that the characteristic peaks of polymer backbone of the CMS-500 membrane still existed, including the benzene ring (C=C, at 1590, 1490, 1460 cm<sup>-1</sup>), aromatic ketone (C=O, at 1650 cm<sup>-1</sup>) and aryl ether (C—O—C, at 1226 cm<sup>-1</sup>), except for the lactone ring (O=C—O, at 1765 cm<sup>-1</sup>) of the pendant cardo group. This result indicated that the polymeric backbone was still prevailing in CMS-500 membrane. For the CMS-600 membrane, however, these peaks were significantly weakened or disappeared, and its configurational organization was in the intermediate state between polymer and carbon [37].

In the range of 650–900 °C, only 5.3% total weight was lost, and H<sub>2</sub> was mainly released, which corresponded to the carbonization or graphitization stage. Aromatic dehydrogenation and condensation reactions might occur during this stage. The intermediate structure gradually turned into the graphite-like structure, which could be confirmed by the FT-IR spectra of CMS membranes. For CMS-700 and CMS-900 membranes, the C—H stretching vibration

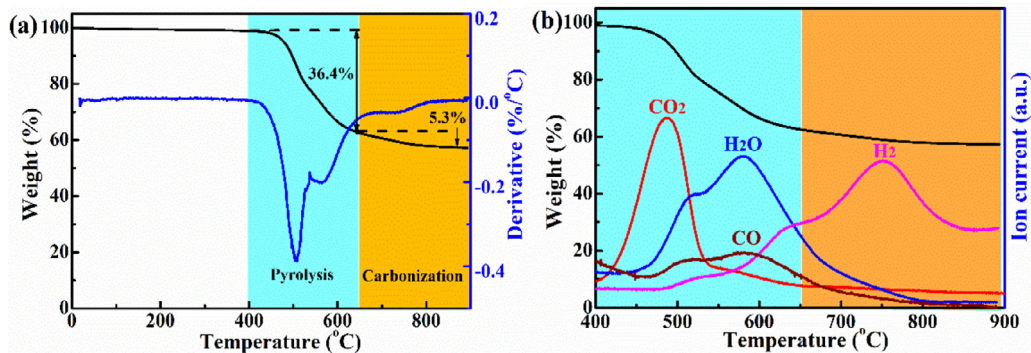


Fig. 2. Thermal decomposition behavior of PEK-C polymeric precursor (a) weight loss curves, (b) TG-MS curves.

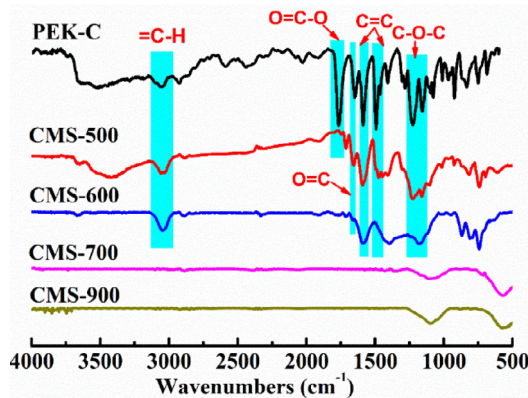


Fig. 3. FT-IR spectra of PEK-C polymeric precursor and CMS membranes.

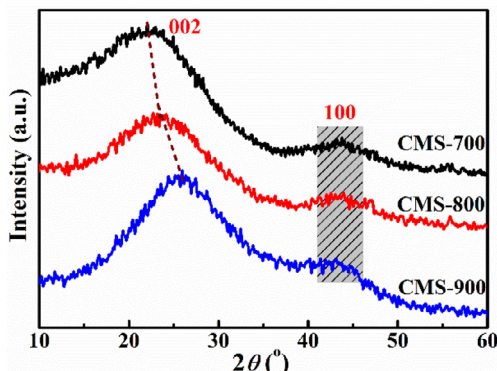


Fig. 4. WAXD patterns of CMS membranes.

peaks of the aromatic ring at 3045 cm<sup>-1</sup> disappeared, and their spectra were consistent with the chemical structure of graphite carbon [38]. Therefore, in this study, the final carbonization temperatures for preparation of CMS membranes were selected within this temperature range.

### 3.2. Microstructure analysis of CMS membranes

Fig. 4 depicts the WAXD patterns of the prepared CMS membranes. There are two broad peaks around the 2θ diffraction angle of 23° and 45°, respectively, indicating that the CMS membranes have an amorphous carbonaceous structure with graphitic-like crystallites stacking [24]. These two peaks correspond to the (002) and (100) plane of the disordered graphite lattice, respec-

**Table 1.** The structural parameters of graphitic crystallites in CMS membranes obtained by the WAXD analysis.

Sample	2θ <sub>(002)</sub> (°)	d <sub>002</sub> (Å) <sup>a</sup>	FWHM <sub>(002)</sub> (°)	2θ <sub>(100)</sub> (°)	La (nm) <sup>b</sup>	Lc (nm) <sup>c</sup>
CMS-700	22.43	3.96	11.68	44.01	2.28	0.69
CMS-800	23.72	3.75	10.62	43.81	2.89	0.76
CMS-900	25.48	3.49	9.75	43.71	3.46	0.83

<sup>a</sup> d<sub>002</sub> is calculated from the (002) peak using the Bragg's law (d<sub>002</sub> = λ/2sinθ, where λ = 1.54 Å).

<sup>b,c</sup> La and Lc are calculated using the Scherrer's equation (L<sub>a/c</sub> = Kλ/β cosθ). Lc is calculated from the (002) peak, where K = 0.89, and β is the FWHM of the (002) peak; La is calculated from the (100) peak, where K = 1.84, and β is the FWHM of the (100) peak.

tively. The structural parameters of the crystallites in CMS membranes can be calculated using the Bragg's law and Scherrer's equation [39], as listed in Table 1. As the carbonization temperature increased, the (002) peak of CMS membrane gradually shifted to the right, and the average interlayer spacing (d<sub>002</sub>) of the graphitic-like crystallite calculated decreased, suggesting the formation of the denser crystallite packing. Nevertheless, the d<sub>002</sub> value of all prepared CMS membranes was higher than that (3.35 Å) of the perfect graphite. For the CMS-900 membrane, however, its d<sub>002</sub> (3.49 Å) was much smaller than the molecular kinetic diameter (3.8 Å) of CH<sub>4</sub> gas, implying the membrane would effectively prevent the diffusion of CH<sub>4</sub>, which could be found in the later section. In addition, the full width at half maximum (FWHM) of the (002) peak decreased with the carbonization temperature, and the estimated crystallite stacking thickness (Lc) and the layer-plane size (La) increased, indicating that more ordered graphitic structures were developed [40]. This phenomenon can also be observed in the TEM images of CMS membranes in Fig. 5. For all the PEK-C based CMS membranes, no large ordered graphitic sheets were observed, but the turbostratic carbon structures were present. As the carbonization temperature increased, carbon sheets tended to align to form ordered structures on a short range and became dense. More ordered domain with parallel carbon sheets could be observed in the CMS-900 membrane. The pore structure of CMS membrane is formed from the imperfect packing of turbostratic carbon sheets [41]. It was obvious to find that the apparent pore size gradually decreased with increasing of the carbonization temperature.

### 3.3. CO<sub>2</sub> sorption isotherms and pore size distributions of CMS membranes

The nanoscale pore structures of CMS membranes are commonly described as slit-like with an idealized bimodal pore size distribution, which consists of the large micropores (7–20 Å) acting as the sorption sites and determining diffusion jump lengths and

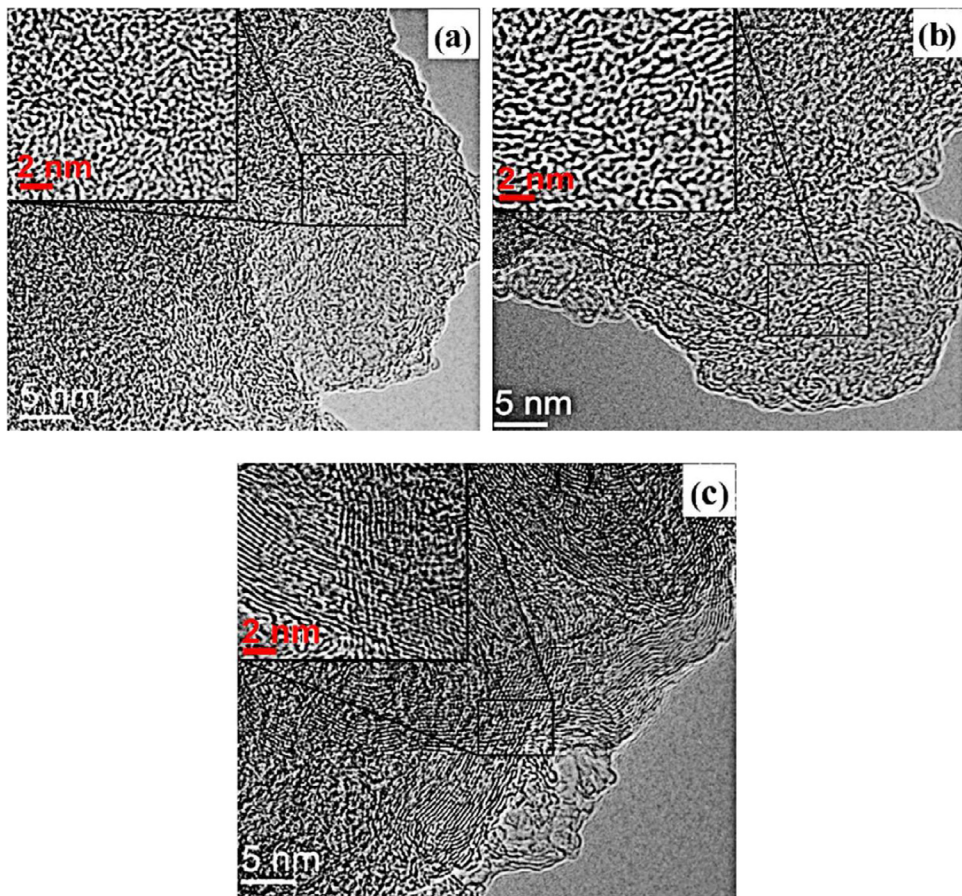


**Fig. 5.** TEM images of (a) CMS-700, (b) CMS-800 and (c) CMS-900 membranes inserted with enhanced images for clarity.

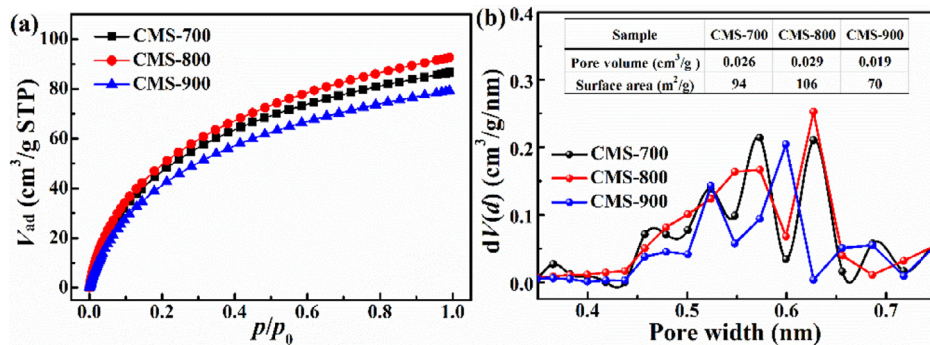


**Fig. 6.** (a)  $\text{CO}_2$  adsorption isotherms of CMS membranes and (b) corresponding pore size and distribution, volume and surface area of pores smaller than  $7 \text{ \AA}$  estimated using the NLDFT method.

the small ultramicropores ( $< 7 \text{ \AA}$ ) providing molecular sieving function of CMS membranes [41]. The smaller  $\text{CO}_2$  gas is often used as a molecular probe to provide an assessment of the ultramicropore size and distribution [40]. The  $\text{CO}_2$  adsorption isotherms of the obtained CMS membranes and the corresponding ultramicropore size and distribution were shown in Fig. 6. As the carbonization temperature increased from  $700^\circ\text{C}$  to  $800^\circ\text{C}$ , the  $\text{CO}_2$  sorption capacity of CMS membrane increased from  $86.6$  to  $92.7 \text{ cm}^3/\text{g}$ , and the associated ultramicropore volume and surface area also increased. This phenomenon can be attributed to an increase in the number of ultramicropores resulting from the shrinkage of micropores [42]. However, when the heating temperature was up to  $900^\circ\text{C}$ , the ultramicropore volume and surface area of CMS membrane were greatly reduced. In addition, an obvious shift in the pore size dis-

tribution toward the smaller ultramicropore was observed. As anticipated, the higher carbonization temperature leads to dense carbon structure and reduced pore size, which will exclude large gas molecule and enhance the molecular sieving performance of CMS membranes.

### 3.4. Gas transport properties of CMS membranes

#### 3.4.1. Single and mixed gas separation performance

The pure gas permeabilities and ideal selectivities of PEK-C based CMS membranes carbonized at different temperature for  $\text{H}_2$ ,  $\text{CO}$ ,  $\text{N}_2$  and  $\text{CH}_4$  were depicted in Fig. 7. The gas permeability decreased in the order of  $P(\text{H}_2) > P(\text{CO}) > P(\text{N}_2) > P(\text{CH}_4)$ , which was in reverse order of molecular size (Table 2), indicating that the gas permeation of CMS membranes was dominated

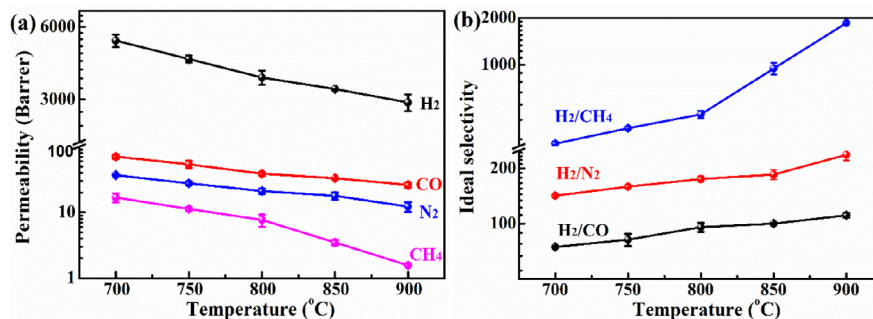


**Fig. 7.** (a) Single gas permeability and (b) ideal selectivity as a function of carbonization temperature (tested at 30 °C and 0.01 MPa).

**Table 2.** Molecular size and critical temperature of H<sub>2</sub>, CO, N<sub>2</sub> and CH<sub>4</sub> gases.

Molecule	Kinetic diameter ( $\times 10^{10}$ m)	Lennard-Jones collision diameter ( $\times 10^{10}$ m)	Critical temperature (K)
H <sub>2</sub>	2.89	2.827	33.2
CO	3.73	3.690	132.9
N <sub>2</sub>	3.64	3.798	126.2
CH <sub>4</sub>	3.80	3.758	190.4

**Table 3.** Mixed gas permeabilities ( $P, \times 10^{-10}$  cm<sup>3</sup>(STP)·cm/cm<sup>2</sup> s cmHg) and selectivities ( $\alpha$ ) of CMS membranes for H<sub>2</sub>/CO, H<sub>2</sub>/N<sub>2</sub> and H<sub>2</sub>/CH<sub>4</sub> (50:50 vol%) gas pairs, and the data in parentheses refer to the corresponding pure gas separation properties for comparison (tested at 30 °C and 0.01 MPa).

Sample	H <sub>2</sub> /CO			H <sub>2</sub> /N <sub>2</sub>			H <sub>2</sub> /CH <sub>4</sub>		
	$P_{H_2}$	$P_{CO}$	$\alpha_{(H_2/CO)}$	$P_{H_2}$	$P_{N_2}$	$\alpha_{(H_2/N_2)}$	$P_{H_2}$	$P_{CH_4}$	$\alpha_{(H_2/CH_4)}$
CMS-700	4697 (5262)	70.4 (70.5)	66.7 (74.6)	4768 (5262)	35.6 (37.1)	134 (142)	4549 (5262)	17.3 (16.9)	263 (311)
CMS-800	3340 (3701)	37.0 (38.7)	90.4 (95.6)	3430 (3701)	20.2 (21.2)	170 (175)	2756 (3701)	10.4 (7.7)	265 (481)
CMS-900	2809 (2919)	27.0 (26.3)	104 (111)	2838 (2919)	13.4 (12.3)	212 (237)	1993 (2919)	1.73 (1.57)	1152 (1859)

by the molecular sieving mechanism [3]. As the pyrolysis temperature increased, the gas permeabilities of all gases were gradually reduced. When the carbonization temperature was raised from 700 to 900 °C, however, the average reduction rate of the gas permeability increased with the increase of gas molecular size, such as H<sub>2</sub> (45%) < CO (63%) < N<sub>2</sub> (67%) < CH<sub>4</sub> (91%), which resulted in a gradual increase in the ideal selectivities for H<sub>2</sub>/CO, H<sub>2</sub>/N<sub>2</sub> and H<sub>2</sub>/CH<sub>4</sub> gas pairs. This result could be attributed to the shrinkage of the pore structure that greatly restricted the diffusion of larger gas molecule into pores. Especially, the CMS-900 membrane exhibited extraordinarily high H<sub>2</sub>/CH<sub>4</sub> selectivity of 1859, which was related to its interlayer spacing being much smaller than the molecular size of CH<sub>4</sub>, as confirmed by the above WAXD results.

To further investigate the applicable feasibility of PEK-C derived CMS membranes, the gas separation performance of the membranes for binary gas mixtures of H<sub>2</sub>/CO, H<sub>2</sub>/N<sub>2</sub> and H<sub>2</sub>/CH<sub>4</sub> (50:50 vol%) were also tested, as shown in Table 3. The mixed-gas H<sub>2</sub> permeability and corresponding selectivity were lower than those obtained in pure-gas experiments tested under the same conditions. This phenomenon can be ascribed to the competitive sorption effect of mixed gases on the fixed Langmuir sorption sites, and the affinity of CO, N<sub>2</sub> and CH<sub>4</sub> for the sorption sites overwhelms H<sub>2</sub>. Similar behavior was also observed in other reported CMS membranes [43]. Surprisingly, CMS-900 membrane still displayed high H<sub>2</sub>/CH<sub>4</sub> selectivity of 1152 in the mixed gas measurements.

#### 3.4.2. Sorption and diffusion coefficients of CMS membranes

Pure gases (H<sub>2</sub>, CO, N<sub>2</sub> and CH<sub>4</sub>) sorption measurements for PEK-C based CMS membranes were conducted at 30 °C to further explore the contributions of gas sorption and diffusion coefficients on the permeabilities and selectivities of these membranes. The sorption isotherms of CMS membranes carbonized at different temperature were shown in Fig. 8. The gas sorption capacities increased in the order of H<sub>2</sub> < N<sub>2</sub> < CO < CH<sub>4</sub>, which corresponded to the gas critical temperature (Table 2). According to the sorp-

**Table 4.** Sorption coefficients ( $S, \text{cm}^3(\text{STP})/\text{cm}^3 \cdot \text{kPa}$ ) and diffusion coefficients ( $D, \times 10^{-8} \text{ cm}^2/\text{s}$ ) of pure gases for CMS membranes carbonized at different temperatures.

Sample	H <sub>2</sub>		N <sub>2</sub>		CO		CH <sub>4</sub>	
	$S$	$D$	$S$	$D$	$S$	$D$	$S$	$D$
CMS-700	0.030	1316	0.118	2.36	0.142	3.72	0.523	0.24
CMS-800	0.034	816	0.129	1.23	0.185	1.57	0.559	0.10
CMS-900	0.028	782	0.103	0.90	0.140	1.41	0.505	0.02

**Table 5.** The sorption selectivities and diffusion selectivities of pure gas pairs H<sub>2</sub>/CO, H<sub>2</sub>/N<sub>2</sub> and H<sub>2</sub>/CH<sub>4</sub> for CMS membranes carbonized at different temperature.

Sample	$\alpha_{(H_2/CO)}$		$\alpha_{(H_2/N_2)}$		$\alpha_{(H_2/CH_4)}$	
	$S_{H_2}/S_{CO}$	$D_{H_2}/D_{CO}$	$S_{H_2}/S_{N_2}$	$D_{H_2}/D_{N_2}$	$S_{H_2}/S_{CH_4}$	$D_{H_2}/D_{CH_4}$
CMS-700	0.211	354	0.254	558	0.057	5483
CMS-800	0.184	520	0.264	663	0.061	8160
CMS-900	0.200	555	0.272	869	0.055	34,000

tion isotherms, the calculated sorption coefficients ( $S$ ) and diffusion coefficients ( $D$ ) of pure gases for CMS membranes were listed in Table 4. As the carbonization temperature increased, the sorption coefficients of all gases slightly increased and then decreased, which was consistent with the changes of the ultramicropore surface area of CMS membranes, while the diffusion coefficients were gradually reduced. Additionally, for all three gas pairs, the diffusion selectivity was the dominant contributor to the overall selectivity, as illustrated in Table 5. The sorption selectivity changed little, while the diffusion selectivity was significantly enhanced with increasing the carbonization temperature. This result is closely related to the shrinkage of the turbostratic carbon structure and the corresponding pore structure.

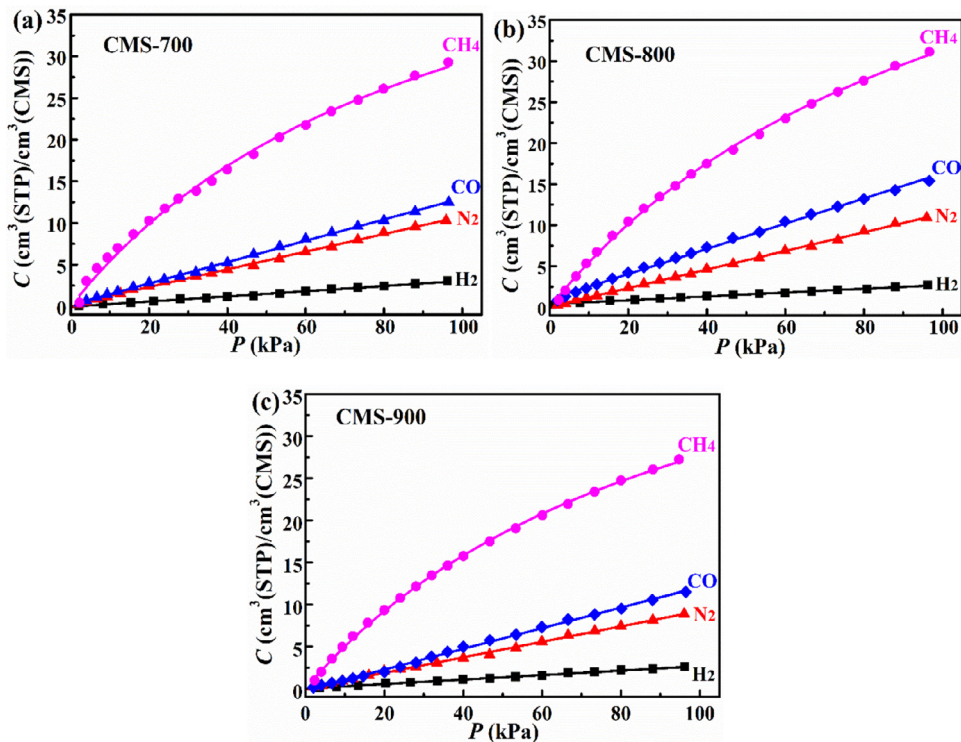


**Fig. 8.** Pure gas sorption isotherms at 30 °C of (a) CMS-700, (b) CMS-800, (c) CMS-900 membranes.

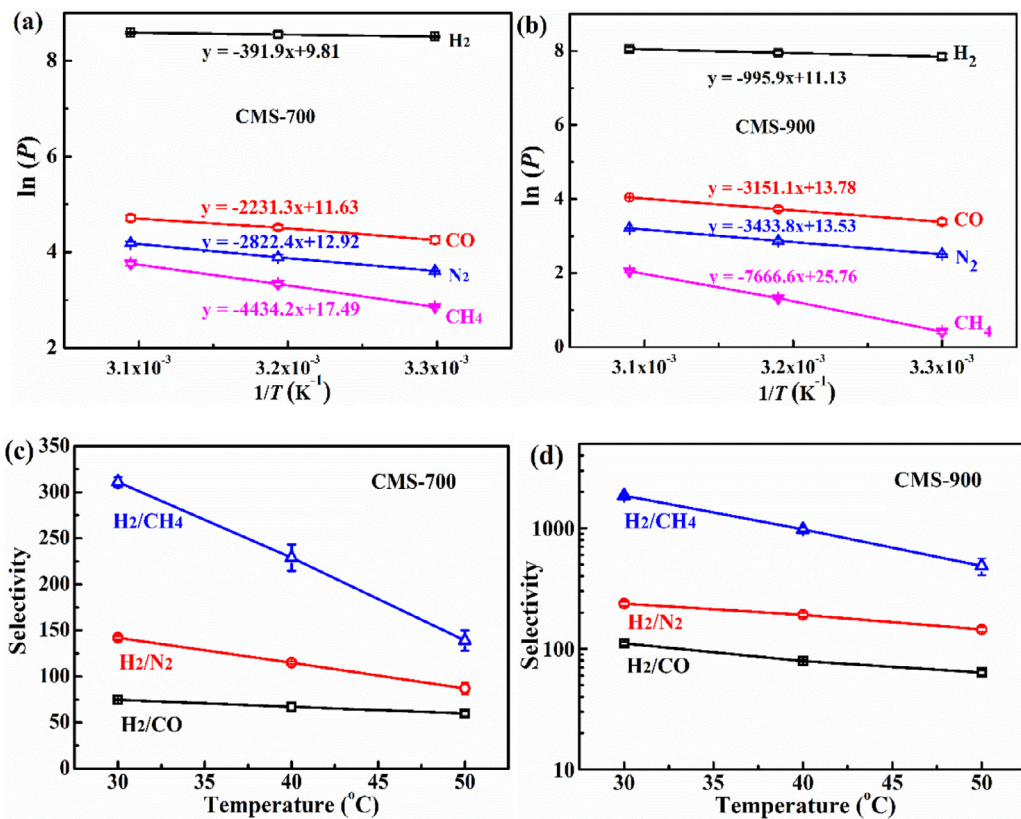


**Fig. 9.** Operating temperature dependence of (a) and (b) permeability, (c) and (d) ideal selectivity in CMS-700 and CMS-900 membranes, respectively.

**Table 6.** The permeation activation energies of various gases in CMS-700 and CMS-900 membranes.

Sample	$E_p$ (kJ/mol)			
	H <sub>2</sub>	CO	N <sub>2</sub>	CH <sub>4</sub>
CMS-700	3.3	18.6	23.5	36.9
CMS-900	8.3	26.2	28.5	63.4

### 3.4.3. Temperature dependence of gas permeation properties in CMS membranes

Operating temperature dependence of pure gas permeabilities and ideal selectivities of four gases for the CMS-700 and CMS-900 membranes at 30–50 °C were investigated. Fig. 9(a,b) exhibits the least squares fit of gas permeability versus inverse absolute temperature. As expected, the permeabilities of all gases increased with increasing operating temperature, suggesting a positive activation energy for permeation. According to the Eq. (1), the gas permeability can be regarded as a combination of the diffusion coefficient and sorption coefficient. The diffusion coefficient always increases with operating temperature due to the positive activation energy of diffusion, while the sorption coefficient decreases because of the negative enthalpy of sorption [44]. Therefore, the contribution of diffusion coefficient on permeability outweighs that of sorption coefficient, which also confirms that the gas permeation of CMS membrane is dominated by diffusion. Owing to the higher temperature dependence of the diffusion coefficient of larger penetrants such as N<sub>2</sub>, CO, and CH<sub>4</sub>, the increasing rates of the permeabilities of these gases with temperature were higher than that of the smaller H<sub>2</sub> gas permeability. As a result, the selectivities of all three gas pairs for both CMS-700 and CMS-900 membranes decreased with an increase in operating temperature (Fig. 9(a,b)). The

permeation activation energies ( $E_p$ ) of four gases were calculated by an Arrhenius equation, as shown in Table 6. It can be found that the  $E_p$  is affected by both the molecular size of penetrant and the carbon structure of CMS membrane. The  $E_p$  increased with the molecular size of penetrant following the order of H<sub>2</sub> < CO < N<sub>2</sub> < CH<sub>4</sub>. On the other hand, compared to the CMS-700 membrane, the  $E_p$  values of the four gases of the CMS-900 membrane were much higher, which was closely related to its denser packing carbon structure that required higher energy to allow gas molecules to penetrate. For example, the highest permeation activation energy of 63.4 kJ/mol was required for the bulky CH<sub>4</sub> to enable pass through the smaller ultramicropores of CMS-900 membranes.

### 3.4.4. Evaluation of gas separation performance

Fig. 10 illustrated the comparison of pure gas separation performance of PEK-C derived CMS membranes with respect to the upper bounds of polymeric membranes and some excellent membranes reported in literature. For H<sub>2</sub>/CH<sub>4</sub> and H<sub>2</sub>/N<sub>2</sub> gas pairs, the separation properties of PEK-C based CMS membranes far exceeded the upper bounds of polymeric membranes in 2008 and 2015 [45,46]. Furthermore, compared with CMS membranes derived from other polymeric precursors, PEK-C derived CMS membranes exhibited higher gas permselectivity. For H<sub>2</sub>/CO gas pair, the gas permselectivities of PEK-C based CMS membranes was higher than that of polymeric membranes reported in literature [5,47], although few CMS membranes had been reported. As the carbonization temperature increased, ultrahigh selectivities for three gas pairs were achieved while maintaining moderate H<sub>2</sub> gas permeabilities. The excellent gas separation performance of the prepared CMS membranes may be attributed to the unique spatial structure of the PEK-C precursor with high FFV and the structural evolution during pyrolysis. It is estimated that the ultrahigh selectivities of PEK-C

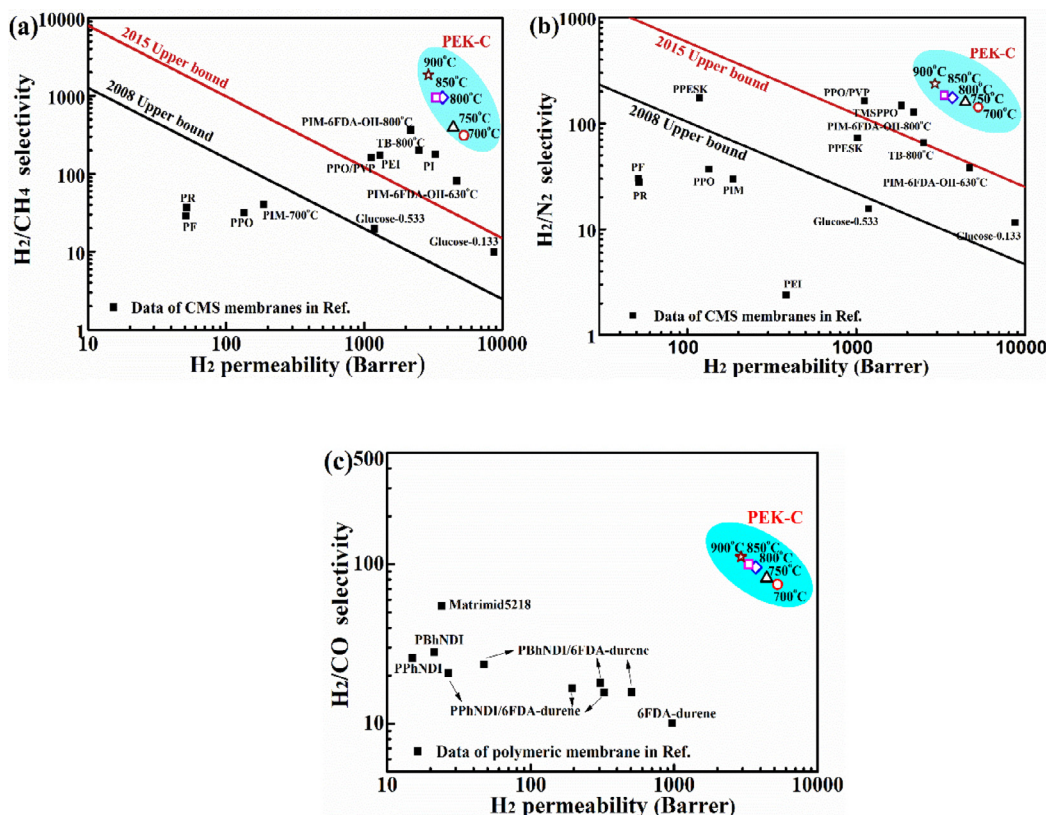


**Fig. 10.** Pure gas separation performance of PEK-C derived CMS membranes against the 2008 and 2015 upper bounds of polymeric membranes for (a) H<sub>2</sub>/CH<sub>4</sub>, (b) H<sub>2</sub>/N<sub>2</sub> and (c) H<sub>2</sub>/CO. Data of CMS and polymeric membranes reported in literature [25,28,30–32,48,49] are selected for comparison.

based CMS membranes for H<sub>2</sub>/CH<sub>4</sub>, H<sub>2</sub>/CO and H<sub>2</sub>/N<sub>2</sub> gas pairs can produce high purity hydrogen, and the high H<sub>2</sub> permeability will achieve competitive separation costs. Therefore, CMS membranes derived from PEK-C polymeric precursor offer great application potential in hydrogen purification.

#### 4. Conclusions

Ultraselective CMS membranes for H<sub>2</sub>/CH<sub>4</sub>, H<sub>2</sub>/CO and H<sub>2</sub>/N<sub>2</sub> binary gas mixtures were formed from PEK-C polymeric precursor at the carbonization temperature of 700–900 °C. WAXD and TEM results showed that the prepared CMS membrane exhibited a turbostratic carbon structure, which gradually became denser and more ordered as the carbonization temperature increased. The gas permeabilities of four gases gradually decreased, while the selectivities greatly increased owing to a substantial enhancement of the diffusion selectivity. The CMS membrane with ultrahigh H<sub>2</sub>/CH<sub>4</sub> selectivity of 1859 was fabricated at 900 °C, and the H<sub>2</sub> permeability was up to 2919 Barrer. The CMS membranes with ultrahigh permselectivity have bright application prospects in the manufacture of high-purity hydrogen.

#### Declaration of Competing Interest

The authors declare that they have no known competing financial interests or personal relationships that could have appeared to influence the work reported in this paper.

#### Acknowledgments

We are very grateful to Dr. Dangsheng Su and his research team for their great help with TEM characterization in past more than ten years. We also thank the National Key R&D Program of China ([2017YFB0603403](#)), National Natural Science Foundation of China ([21676044](#), [21878033](#), [21978034](#)), High Level Innovation Team of Liaoning Province ([XLYC1908033](#)) and Fundamental Research Funds for the Central Universities ([DUT19ZD211](#), [DUT 2018TB02](#)) for the financial support.

#### References

- [1] G.W. Crabtree, M.S. Dresselhaus, *MRS Bull.* 33 (2011) 421–428.
- [2] W. Salim, Y. Han, V. Vakharia, D. Wu, D.J. Wheeler, W.S.W. Ho, *J. Membr. Sci.* 573 (2019) 465–475.
- [3] N.W. Ockwig, T.M. Nenoff, *Chem. Rev.* 107 (2007) 4078–4110.
- [4] J. Dong, Y.S. Lin, M. Kanezashi, Z. Tang, *J. Appl. Phys.* 104 (2008).
- [5] O.C. David, D. Gorri, A. Urtiaga, I. Ortiz, *J. Membr. Sci.* 378 (2011) 359–368.
- [6] R. Razzaq, C. Li, S. Zhang, *Fuel* 113 (2013) 287–299.
- [7] Z. Yang, Y. Zhang, X. Wang, W. Ding, *J. Energy Chem.* 23 (2014) 411–413.
- [8] P. Li, Z. Wang, Z. Qiao, Y. Liu, X. Cao, W. Li, J. Wang, S. Wang, *J. Membr. Sci.* 495 (2015) 130–168.

- [9] X. Wu, S.F. Wu, *J. Energy Chem.* 24 (2015) 315–321.
- [10] Y. Liu, S. Xiao, P. Bai, H. Hu, L. Jin, *J. Energy Chem.* 23 (2014) 213–220.
- [11] L. Shao, B.T. Low, T.-S. Chung, A.R. Greenberg, *J. Membr. Sci.* 327 (2009) 18–31.
- [12] X. He, *Sep. Purif. Technol.* 186 (2017) 117–124.
- [13] W.N.W. Salleh, A.F. Ismail, T. Matsuura, M.S. Abdullah, *Sep. Purif. Rev.* 40 (2011) 261–311.
- [14] W.N.W. Salleh1, A.F. Ismail, *J. Membr. Sci. Res.* 1 (2015) 2–15.
- [15] J.B.S. Hamm, A. Ambrosi, J.G. Griebeler, N.R. Marcilio, I.C. Tessaro, L.D. Pollo, *Int. J. Hydrogen Energy* 42 (2017) 24830–24845.
- [16] D. Grainger, M. Hagg, *Int. J. Hydrogen Energy* 33 (2008) 2379–2388.
- [17] J.S. Adams, A.K. Itta, C. Zhang, G.B. Wenz, O. Sanyal, W.J. Koros, *Carbon N Y* 141 (2019) 238–246.
- [18] C.-P. Hu, C.K. Polintan, L.L. Tayo, S.-C. Chou, H.-A. Tsai, W.-S. Hung, C.-C. Hu, K.-R. Lee, J.-Y. Lai, *Carbon N Y* 143 (2019) 343–351.
- [19] C. Karunaweera, I.H. Musselman, K.J. Balkus, J.P. Ferraris, *J. Membr. Sci.* 581 (2019) 430–438.
- [20] S. Fu, E.S. Sanders, S.S. Kulkarni, W.J. Koros, *J. Membr. Sci.* 487 (2015) 60–73.
- [21] S. Fu, G.B. Wenz, E.S. Sanders, S.S. Kulkarni, W. Qiu, C. Ma, W.J. Koros, *J. Membr. Sci.* 520 (2016) 699–711.
- [22] M. Rungta, L. Xu, W.J. Koros, *Carbon N Y* 85 (2015) 429–442.
- [23] X. Ning, W.J. Koros, *Carbon N Y* 66 (2014) 511–522.
- [24] K. Hazazi, X.H. Ma, Y.G. Wang, W. Ogieglo, A. Alhazmi, Y. Han, I. Pinna, *J. Membr. Sci.* 585 (2019) 1–9.
- [25] M.-Y. Wey, H.-H. Tseng, C.-k. Chiang, *J. Membr. Sci.* 446 (2013) 220–229.
- [26] B. Zhang, X. Dang, Y. Wu, H. Liu, T. Wang, J. Qiu, *J. Mater. Res.* 29 (2014) 2881–2890.
- [27] C. Song, T. Wang, H. Jiang, X. Wang, Y. Cao, J. Qiu, *J. Membr. Sci.* 361 (2010) 22–27.
- [28] T.-H. Weng, H.-H. Tseng, G.-L. Zhuang, M.-Y. Wey, *Int. J. Hydrogen Energy* 38 (2013) 3092–3104.
- [29] S.L. Liu, T.H. Wang, Q.L. Liu, S.H. Zhang, Z.C. Zhao, C.H. Liang, *Ind. Eng. Chem. Res.* 47 (2008) 876–880.
- [30] T.H. Wang, B. Zhang, J.S. Qiu, Y.H. Wu, S.H. Zhang, Y.M. Cao, *J. Membr. Sci.* 330 (2009) 319–325.
- [31] X. Ma, R. Swaidan, B. Teng, H. Tan, O. Salinas, E. Litwiller, Y. Han, I. Pinna, *Carbon N Y* 62 (2013) 88–96.
- [32] X. Chen, J.J. Eugene Chong, Z.W. Celine Fah, L. Hong, *Carbon N Y* 111 (2017) 334–337.
- [33] R. Xu, L. Li, X. Jin, M. Hou, L. He, Y. Lu, C. Song, T. Wang, *J. Membr. Sci.* 586 (2019) 306–317.
- [34] W. Qiu, J. Vaughn, G. Liu, L. Xu, M. Brayden, M. Martinez, T. Fitzgibbons, G. Wenz, W.J. Koros, *Angew. Chem. Int. Ed. Engl.* 58 (2019) 11700–11703.
- [35] L. Xu, M. Rungta, J. Hessler, W. Qiu, M. Brayden, M. Martinez, G. Barbay, W.J. Koros, *Carbon N Y* 80 (2014) 155–166.
- [36] L. Li, T.H. Wang, Q.L. Liu, Y.M. Cao, J.S. Qiu, *Carbon N Y* 50 (2012) 5186–5195.
- [37] L. Shao, T.-S. Chung, K.P. Pramoda, *Microporous Mesoporous Mater.* 84 (2005) 59–68.
- [38] W. Ma, J. Zhou, S. Cheng, *J. Chem. Eng. Chin. Univ.* 24 (2010) 719–722.
- [39] M.A. Short, P.L. Walker, *Carbon N Y* 1 (1963) 3–9.
- [40] K. Hazazi, X. Ma, Y. Wang, W. Ogieglo, A. Alhazmi, Y. Han, I. Pinna, *J. Membr. Sci.* 585 (2019) 1–9.
- [41] M. Rungta, G.B. Wenz, C. Zhang, L. Xu, W. Qiu, J.S. Adams, W.J. Koros, *Carbon N Y* 115 (2017) 237–248.
- [42] K.M. Steel, W.J. Koros, *Carbon N Y* 43 (2005) 1843–1856.
- [43] R. Swaidan, X. Ma, E. Litwiller, I. Pinna, *J. Membr. Sci.* 447 (2013) 387–394.
- [44] S. Fu, E.S. Sanders, S.S. Kulkarni, G.B. Wenz, W.J. Koros, *Carbon N Y* 95 (2015) 995–1006.
- [45] L.M. Robeson, *J. Membr. Sci.* 320 (2008) 390–400.
- [46] R. Swaidan, B. Ghanem, I. Pinna, *ACS Macro Lett.* 4 (2015) 947–951.
- [47] S. Yu, C.-S. Lim, B. Seo, *J. Ind. Eng. Chem.* 62 (2018) 197–208.
- [48] Z. Wang, H. Ren, S. Zhang, F. Zhang, J. Jin, *ChemSusChem* 11 (2018) 916–923.
- [49] W. Ogieglo, A. Furchner, X. Ma, K. Hazazi, A.T. Alhazmi, I. Pinna, *ACS Appl. Mater. Interfaces* 11 (2019) 18770–18781.